Hierarchical Control Design for a Helicopter-Payload System for Water Monitoring

Published Version:
Bertolani, G., De Angelis, E.L., Giulietti, F. (2024). Hierarchical Control Design for a Helicopter-Payload System for Water Monitoring. 345 E 47TH ST, NEW YORK, NY 10017 USA : Institute of Electrical and Electronics Engineers Inc. [10.1109/ICUAS60882.2024.10556827].

Availability:
This version is available at: https://hdl.handle.net/11585/1015355 since: 2025-05-08

Published:
DOI: http://doi.org/10.1109/ICUAS60882.2024.10556827

Hierarchical control design for a helicopter-payload system for water monitoring

Giulia Bertolani[1], Emanuele Luigi de Angelis[2], and Fabrizio Giulietti[3]

Abstract—**The integration of helicopters with payloads for environmental monitoring applications presents a unique set of challenges. This paper proposes a hierarchical control scheme designed to address the complexities inherent in controlling a system composed of a helicopter and a payload dragged into water through a cable. The hierarchical architecture consists of multiple layers, each responsible for different aspects of control, including precise trajectory tracking, payload and helicopter control. At the higher level, a waypoints tracking controller generates reference velocities for the mid-loop. The intermediate level comprises a PID plus sliding mode control strategy tailored to ensure reference speed tracking for both the payload and the helicopter. The inner loop regulates the helicopter's attitude, maintaining its stability while moving the payload into the water. The effectiveness of the proposed hierarchical control scheme is validated through simulations. Results demonstrate waypoints tracking accuracy, thereby enabling more reliable and efficient monitoring missions in aquatic environment. By proposing a hierarchical control scheme for a helicopter-payload system, this research contributes to the advancement on the use of UAVs for environmental monitoring, introducing the use for small-scale helicopters in water quality monitoring.**

Index Terms—**Helicopter, suspended payload, environmental monitoring, water management, hierarchical control system.**

I. Introduction

Environmental monitoring plays a pivotal role in our efforts to understand and manage the health and sustainability of natural ecosystems [1]. The collection of timely and accurate environmental data is essential for informed decision-making and effective conservation strategies. In particular, water resource management is essential nowadays, given the rapid development of industry and agriculture. Programs for monitoring water quality have been created to protect it and stop water sources from becoming contaminated. Maps showing the distribution of water quality throughout a body of water can be made using data from indicators of water quality. Hydrologists use these maps to comprehend the waterbody's circulation and forecast [2]. Traditionally, water quality monitoring agencies have collected and analyzed water samples in a laboratory to identify any hazardous changes that may have occurred in the waterbodies. The measures are not typical of the nearby waterbodies, and these techniques are expensive and labor-intensive [3]. In addition, it may be necessary to install wireless sensors and stations directly in water bodies [4], [5]. The fixed position of the sensors, however, limits the technique and only allows for a restricted amount of spatial coverage. Remotely operated boats fitted with sensors can be used to cover more sampling space. There are certain drawbacks in this technique as well. For example, obstructions in the water, such boulders, floating debris, and aquatic vegetation, might make it more difficult for unmanned boats to move around and collect samples, which raises operating risks. Human safety during the collection of water samples may be at risk in lakes experiencing blooms of cyanobacteria, or blue-green algae. Moreover, accurately sampling water quality can be difficult in high currents since they can impact the stability of unmanned boats. Additionally, some lakes or water zones may not be accessible by boats due to steep and difficult terrain or retired mining zones [6].

In recent years, the utilization of unmanned aerial vehicles (UAVs) has emerged as a promising approach for conducting monitoring tasks in diverse and challenging water [7]–[9]. It is possible to install a variety of sensors that offer data for tracking the conditions of air, water, and coasts. These include thermal infrared sensors, multispectral sensors, and remote sensing techniques [10]–[12]. Careful trajectory planning leads to a more effective use of vehicles in monitoring duties, particularly when scanning potentially large areas with different sensors or when visiting a relevant number of waypoints is necessary [13]–[15]. Examples of the use of multi-rotor platforms to measure water qualities are found in [16], [17]. In these works, the authors presented the integration of sensors for water monitoring with UAVs multi-rotor platforms and the development of path-tracking systems.

The integration of helicopters with payloads for environmental monitoring applications presents a unique set of challenges. This kind of configuration has been already adopted for in situ measurements [18] and in military applications like in anti-submarine warfare, where a sonar is towed by a helicopter [13], [19].

The dynamics and control of helicopter-slung load systems constitute a complex and multifaceted scenario for helicopter pilots in operations as well as flight dynamicists in theoretical modeling. To guarantee safe, productive, and mission-effective operations across multiple domains, it is essential to comprehend the complexity of these systems. To accurately anticipate the dynamic behavior and potential performance constraints, it is essential to have a robust model

[1]Giulia Bertolani, Department of Industrial Engineering, University of Bologna, 47121 Forlı', Italy giulia.bertolani2@unibo.it

[2]Emanuele Luigi de Angelis, Department of Industrial Engineering, University of Bologna, 47121 Forlı', Italy emanuele.deangelis4@unibo.it

[3]Fabrizio Giulietti, Department of Industrial Engineering, University of Bologna, 47121 Forlı', Italy fabrizio.giulietti@unibo.it

that accurately represents the interconnected dynamics of the vehicle, cable, and load, along with appropriate analysis tools. A lot of research has recently been done on controller designs and modeling for helicopters with slung loads [20]–[24]. Nevertheless, modeling and control system design for a helicopter towing a submerged payload is a relatively unexplored field. In [13] the authors proposed an inverse simulation-based method for determining the control action on the helicopter that causes the sonar to follow almost exactly a prescribed path at a designated depth. In [18] a vision-based helicopter system is used to perform different in situ measurement tasks, covering a wide range of applications.

This paper focuses on the design and implementation of hierarchical control architecture for helicopter-payload systems employed in environmental monitoring missions in aquatic environments. A sketch of the system is given in Fig. 1.

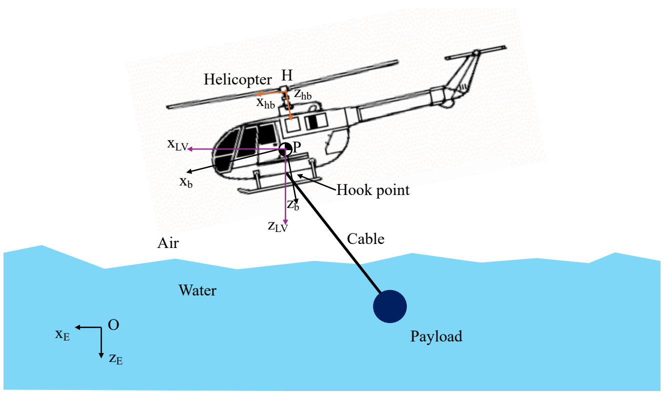

Fig. 1: System sketch

The primary objective of this work is to develop robust control algorithms capable of optimizing the performance and maneuverability of the helicopter-payload system while ensuring precise trajectory tracking and data acquisition. Through a combination of theoretical analysis and simulation studies, the authors endeavor to demonstrate the efficacy and practical feasibility of the proposed control architecture in enhancing the capabilities of helicopter-based environmental monitoring systems. In particular, different control strategies have been integrated into the control structure and its performance has been analysed with proper defined performance indexes. The main goal of the controller is to assure a precise tracking of pre-established waypoints for the submerged payload. To this aim, the outer control loop is a proportional-integral (PI) controller, while the mid-loop is a combined action of proportional-integral-derivative (PID) controller with Sliding Mode Control (SMC) technique. The inner loop, responsible for the helicopter attitude control, uses a cascade P-PI controller. The hierarchical part of the control scheme is based on [25]. The control scheme of the work [25] has been rearranged and adapted to control a payload in position and speed, instead of a large helicopter, while keeping a control loop on helicopter speed and attitude. The approach is presented in discussed later in the paper. The paper presents a mathematical modeling of a UAV-payload system composed by a small-scale remotely piloted helicopter, a rigid cable and a submerged payload.

In section II the primary physical model of the system that is utilized in the simulation is presented. Then the control system architecture is depicted in section III. The simulation results of the suggested integrated hierarchical design in different maneuvers are shown in section IV. A final section V of conclusions ends this work.

II. System mathematical model

The main hypotheses concerning the helicopter-payload system are the following: (1) The helicopter has 9 Degrees Of Freedom (DOF), 6 DOF of the body dynamics and 3 DOF of the flapping dynamics; (2) the payload is modeled as a point mass with spherical pendulum behaviour. Only its position is considered in the kinematics equations; (3) the cable is assumed elastic, with negligible mass and the hook point C is located in a different point with respect to the helicopter center of gravity. With the payload being significantly lighter than the helicopter, the previous hypotheses are supported, and the effects of payload in terms of forces involved are taken into account. The maneuvers considered are not aggressive.

A. Reference frames

The following right-handed orthogonal reference frames are given and depicted in Fig. 1, namely: NED, Hub-Wind, Hub-Body, Body and Local-Vertical:

1) Earth-fixed North–East-Down (NED) frame, $\mathbb{F}_E = \{O; \boldsymbol{x}_E, \boldsymbol{y}_E, \boldsymbol{z}_E\}$. The origin is arbitrary, set to a location on the surface of the Earth. $\boldsymbol{x}_E$ points in the direction of geodetic North, $\boldsymbol{z}_E$ points downward along the Earth ellipsoid normal, and $\boldsymbol{y}_E$ completes the right-handed triad.
2) Hub-Wind frame $\mathbb{F}_{hw} = \{H; \boldsymbol{x}_{hw}, \boldsymbol{y}_{hw}, \boldsymbol{z}_{hw}\}$. The rotor hub is the origin. $\boldsymbol{z}_{hw}$ is oriented to point downward and in line with the rotor shaft. $\boldsymbol{x}_{hw}$, orthogonal to $\boldsymbol{z}_{hw}$, is aligned with the component of relative wind perpendicular to the shaft axis. $\boldsymbol{y}_{hw}$ axis completes the right-handed orthogonal set.
3) Hub-Body frame $\mathbb{F}_{hb} = \{H; \boldsymbol{x}_{hb}, \boldsymbol{y}_{hb}, \boldsymbol{z}_{hb}\}$. $\boldsymbol{z}_{hb}$ axis is aligned with rotor shaft, pointing downward. This system coincides with the hub-wind system when the sideslip angle β_w is zero.
4) Body-Fixed frame $\mathbb{F}_b = \{P; \boldsymbol{x}_b, \boldsymbol{y}_b, \boldsymbol{z}_b\}$. The centre of gravity of the rotorcraft is the origin. $\boldsymbol{x}_b$ axis is positive out of the nose of the rotorcraft in its plane of symmetry, $\boldsymbol{z}_b$ is perpendicular to $\boldsymbol{x}_b$ in the same plane of symmetry, pointing downward, and $\boldsymbol{y}_b$ axis completes the right-handed system.
5) Local Vertical frame $\mathbb{F}_{LV} = \{P; \boldsymbol{x}_{LV}, \boldsymbol{y}_{LV}, \boldsymbol{z}_{LV}\}$. Origin is at the centre of gravity of rotorcraft and axes are parallel to the inertial frame.

B. Equations of motion

System dynamics is described by Newton-Euler equations of motion.

Let $\boldsymbol{V}_h$ be the helicopter velocity vector in body frame, m_h the helicopter mass, $\boldsymbol{\Omega}_h = [p, q, r]^T$ is the helicopter angular velocity vector, and $\boldsymbol{I}_h$ is the inertia tensor of the helicopter. Specifically, the equations of motion for the helicopter in body frame $\mathbb{F}_b$ are:

$$\dot{\boldsymbol{V}}_h = -\boldsymbol{\Omega}_h \times \boldsymbol{V}_h + \boldsymbol{F}_h^{(e)}/m_h \tag{1}$$

$$\dot{\boldsymbol{\Omega}}_h = \boldsymbol{I}_h^{-1}[-\boldsymbol{\Omega}_h \times (\boldsymbol{I}_h \boldsymbol{\Omega}_h) + \boldsymbol{M}_h^{(e)}] \tag{2}$$

$\boldsymbol{F}_h^{(e)}$ and $\boldsymbol{M}_h^{(e)}$ are the aircraft external forces and moments, respectively. Rigid-body kinematics is given by:

$$\begin{bmatrix} \dot{\phi} \\ \dot{\theta} \\ \dot{\psi} \end{bmatrix}_h = \begin{bmatrix} 1 & \sin\phi \tan\theta & \cos\phi \tan\theta \\ 0 & \cos\phi & -\sin\phi \\ 0 & \sin\phi / \cos\theta & \cos\phi / \cos\theta \end{bmatrix} \boldsymbol{\Omega}_h \tag{3}$$

$$\begin{bmatrix} \dot{x}_h & \dot{y}_h & \dot{z}_h \end{bmatrix}^T = \Pi_{be}^{-1} \begin{bmatrix} u & v & w \end{bmatrix}_h^T \tag{4}$$

provided Π_{be}^{-1} being the rotation matrix between NED and Body frames.

Let $\boldsymbol{V}_p$ be the payload velocity vector, m_p the payload mass and $\boldsymbol{d}$ be the the coordinates of the hook point C of the cable in body reference frame. Payload dynamic is described by the following equations projected in NED reference frame $\mathbb{F}_E$:

$$m_p \dot{\boldsymbol{V}}_p^E = \boldsymbol{F}_{pE}^{(e)} = \boldsymbol{F}_{pE}^g + \boldsymbol{F}_{pE}^D + \boldsymbol{F}_{pE}^c + \boldsymbol{F}_{pE}^{buoyancy} \tag{5}$$

where $\boldsymbol{F}_{pE}^{(e)}$ is the payload external force vector, namely: $\boldsymbol{F}_{pE}^g = \begin{bmatrix} 0 & 0 & m_p g \end{bmatrix}^T$ is the gravity vector, $\boldsymbol{F}_{pE}^D$ is the hydrodynamic drag force vector, $\boldsymbol{F}_{pE}^c$ is the force that the aircraft applies on the load through the cable with Hooke's constant $K > 0$ and nominal length L, $\boldsymbol{F}_{pE}^{buoyancy}$ is the buoyancy force vector. This last force vector is described by Archimede's principle [26]. Payload rigid-body kinematics is described by equations 6:

$$\begin{bmatrix} \dot{x}_{pE} & \dot{y}_{pE} & \dot{z}_{pE} \end{bmatrix}^T = \begin{bmatrix} u & v & w \end{bmatrix}_p^{ET} \tag{6}$$

C. Helicopter forces and moments

The helicopter external force vector is made of aerodynamic $\boldsymbol{F}_h^{(a)}$, gravity $\boldsymbol{F}_h^{(g)}$ and cable $\boldsymbol{F}_h^{(c)}$ contributions, whereas total moment vector includes aerodynamic $\boldsymbol{M}^{(a)}$ effect and the cable contribution $\boldsymbol{M}^{(c)}$. The vector of gravity force in body frame is $\boldsymbol{F}_h^{(g)} = \Pi_{be} \begin{bmatrix} 0 & 0 & mg \end{bmatrix}^T$

The cable contribution is described in equation 15. This vector force is rotated in the body frame through the rotation matrix Π_{be}:

$$\boldsymbol{F}_h^{(c)} = \Pi_{be} \boldsymbol{F}_{hE}^{(c)} \tag{7}$$

The aerodynamic forces and moments of the helicopter are modelled according to Ref. [27]. These effects are expressed as the sum of aircraft components contributions, that for a small-scale platform are the main rotor, the tail rotor and the fuselage:

$$\boldsymbol{F}_h^{(a)} = \boldsymbol{F}_h^{(MR)} + \boldsymbol{F}_h^{(FUS)} + \boldsymbol{F}_h^{(TR)} \tag{8}$$

$$\boldsymbol{M}_h^{(a)} = \boldsymbol{M}_h^{(MR)} + \boldsymbol{M}_h^{(FUS)} + \boldsymbol{M}_h^{(TR)} \tag{9}$$

Concerning the helicopter main rotor model, the following hypotheses are made:

1) Blade flow stall is not taken into consideration, as well as compressibility;
2) Rotor blades are rigid in torsion and bending;
3) Blade twist is assumed linear;
4) Uniform inflow assumption, based on Pitt-Peters [28]
5) Flapping angles are small and the simple strip theory is applied [29]
6) Blade flapping is approximated by the first harmonic terms with time-varying coefficients, that is:

$$\beta(t) = a_0 - a_1 \cos\xi - b_1 \sin\xi \tag{10}$$

where a_0, a_1, b_1 are coning, longitudinal and lateral flapping angles and ξ is blade azimuth.

Using momentum theory and analytical integration over the radius, blade forces are calculated based on the aforementioned hypotheses. In Ref. [27] detailed formulas for calculating main rotor forces and moments are given. The thrust calculation requires knowledge of the rotor inflow ratio. In this work the authors implemented the Pitt-Peters dynamic inflow model [28], that in the wind-hub reference frame is:

$$\frac{d}{dt} = \begin{pmatrix} \lambda_0 \\ \lambda_s \\ \lambda_c \end{pmatrix} = \Omega_h \mathbb{M}^{-1} (-(\mathbb{L}_1 \mathbb{L}_2)^{-1} \begin{pmatrix} \lambda_0 \\ \lambda_s \\ \lambda_c \end{pmatrix} + \boldsymbol{C}_{aero}) \tag{11}$$

with $\lambda_s = \lambda_c = 0$ just taking the uniform inflow component into consideration (λ_0). The equations for the matrices $\boldsymbol{C}_{aero}$, $\mathbb{M}$, $\mathbb{L}_1, \mathbb{L}_2$ are given in [28]. The total inflow λ is:

$$\lambda = \frac{w_{hH}}{\Omega_h R_h} - \lambda_0 \tag{12}$$

where w_{hH} is the helicopter vertical velocity component in the Hub-Wind reference frame, Ω_h the MR rotational speed and R_h the MR radius. The rotor-induced velocity at the disk is calculated using the formula:

$$v_{hi} = (\frac{w_{hH}}{\Omega_h R_h} - \lambda) \Omega_h R_h \tag{13}$$

Chen goes into detail about the tip-path plane dynamic equations derivation in [30] .

The tail rotor is modeled in accordance with the Ref. [27]. The tail rotor tip-path plane dynamics are ignored, provided that the flapping frequency is significantly higher than that of the main rotor system. Solutions with a steady state include forces, moments, and flapping angles.

The fuselage is represented as a virtual flat plate drag source having three dimensions [31]. Forces and moments are evaluated as functions of the helicopter angle of attack and of the sideslip angle.

D. Payload forces

The hydrodynamic force acting on the payload is described by the following equation:

$$\boldsymbol{F}_{pE}^{D} = -\frac{1}{2}\rho A_p C_{Dp} ||\boldsymbol{V}_p^E|| \boldsymbol{V}_p^E \tag{14}$$

where C_{Dp} is the payload drag coefficient, ρ in this case is the water density, A_p is the reference area for calculating drag. $\boldsymbol{F}_{pE}^{c}$ force vector is written according to Hooke's law:

$$\boldsymbol{F}_{pE}^{c} = -K\Delta L\hat{\boldsymbol{c}}_E = -\boldsymbol{F}_{hE}^{(c)} \tag{15}$$

with the elastic deformation $\Delta L = ||\boldsymbol{c}_E|| - L$ and $\hat{\boldsymbol{c}}_E = \frac{\boldsymbol{c}_E}{||\boldsymbol{c}_E||}$. The buoyancy force is written in accordance to Archimede's principle:

$$\boldsymbol{F}_{pE}^{buoyancy} = \rho g \frac{4\pi Rp^3}{3} \tag{16}$$

where the density ρ is that one of water and Rp is the payload radius.

III. Control system architecture

The architecture of the proposed controller is shown in Fig. 2. It consists in a hierarchical control system configuration, whose main task is to provide accurate tracking of the payload's intended waypoints. When managing complex systems, the hierarchical architecture is frequently employed for the design to be more straightforward. There are three control levels for this application.

Starting from the outer one, it consists in the payload position controller and it is labeled as "Waypoints Controller" in Fig. 2. It is organized specifically as a waypoint controller. In this manner, the operator requests that the controller precisely place the payload in a desired waypoint. A proportional-integral (PI) controller is responsible for the waypoints tracking. It will be discussed in section III-A. The mid loop is a speed control, which receives the reference speed from the position controller and generates reference attitude angles for the helicopter, considering the velocities of both the helicopter and the payload. In Fig. 2 it is labeled "Speed Controller" and It is going to be covered in section III-B. The inner level is responsible for helicopter attitude control and is made up of two sub-layers, a proportional control (P) that controls attitude angles and provides reference angular speed to the second layer, which consists of an angular speeds controller which is a proportional-integral controller (PI), as presented in [25]. This topic is covered in section III-C and it is marked as "Attitude Controller" in Fig. 2.

A. Position controller

Position controller is a proportional-integral (PI) control on payload position. Control scheme is given in Fig. 3.

It receives the desired waypoints from the operator and generates the vector of reference velocities in NED reference frames for the payload speed controller, namely $[\boldsymbol{v}_{pN}, \boldsymbol{v}_{pE}, \boldsymbol{v}_{pD}]_{ref}$. By doing this, the operator can ensure accurate tracking of the desired payload position, which in the case of water quality measurements ensures an accurate positioning of the sensor for data acquisition.

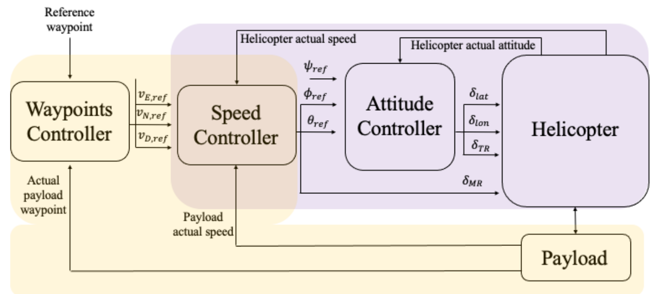

Fig. 2: Control system architecture

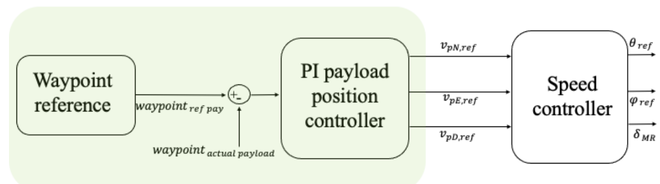

Fig. 3: Payload position controller

B. Speed controller

Speed controller receives the reference signal from the position controller and generates the reference attitude for the helicopter. This loop is a mixed combination of proportional-integral-derivative (PID) technique and Sliding Mode Control technique (SMC). The architecture is reported in Fig. 4.

The speed controller is articulated as a double loop on speed. The outer one receives the reference speed in NED frame, that is converted in LV reference frame. This velocity is the reference one for the PI controller on payload speed. The output of this PI controller is summed to the reference speed itself (in LV frame) and given as reference input velocity to the speed controller of the helicopter.

The inner loop of the speed controller includes a SMC for horizontal and lateral speed control of the helicopter, with the same design features presented in Ref. [25] and depicted in Fig. 4a, 4b. On the helicopter vertical speed there is a PID control, as shown in Fig. 4c.

Pitch and roll references for the attitude controller are generated by the SMC. SMC control theory is explained in Ref. [25]. For this aim, the sliding surfaces listed below have been chosen:

$$\sigma = \begin{bmatrix} v_l + \lambda_l \int_0^t (v_l - v_{lr})\, d\tau \\ v_h + \lambda_h \int_0^t (v_h - v_{hr})\, d\tau \end{bmatrix} \tag{17}$$

Such sliding surfaces characterize the desired lateral and horizontal speed dynamics that the helicopter has to follow.

Accelerations a_{forw} (forward) and a_{lat} (lateral) are reported:

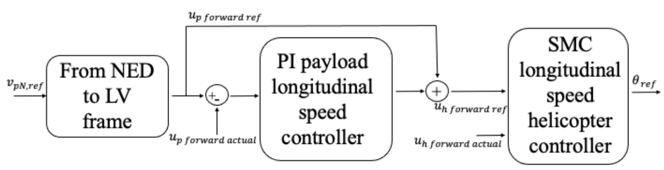

(a) Longitudinal speed controller

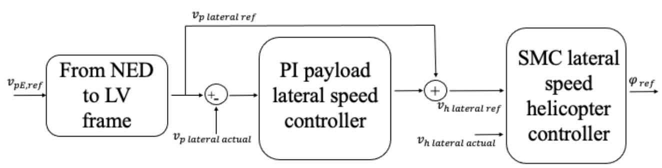

(b) Lateral speed controller

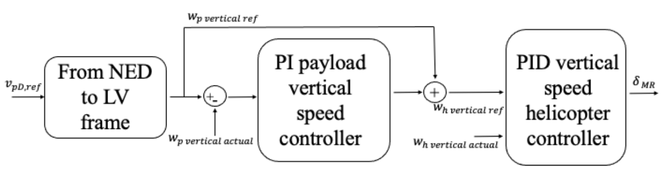

(c) Vertical speed controller

Fig. 4: Speed controller

$$\begin{pmatrix} a_{lat} \\ a_{forw} \end{pmatrix} = \begin{bmatrix} \frac{g}{cos(\theta)} & 0 \\ gtan\,(\theta)\,tan\,(\phi) & -g \end{bmatrix} \begin{pmatrix} \Delta\phi \\ \Delta\theta \end{pmatrix} \tag{18}$$

which can be rewritten as:

$$\begin{pmatrix} \dot{v}_{lat} \\ \dot{v}_{forw} \end{pmatrix} = G \begin{pmatrix} \Delta\phi \\ \Delta\theta \end{pmatrix} \tag{19}$$

The matrices $\bar{A}$, $\bar{B}$, $\bar{T}$ and S are the following:

$$\bar{A} = \begin{bmatrix} 0_{2\times2} & I_2 \\ 0_{2\times2} & 0_{2\times2} \end{bmatrix}; \bar{B} = \begin{bmatrix} 0_{2\times2} \\ G \end{bmatrix}$$
$$\bar{T} = \begin{bmatrix} I_2 \\ 0_{2\times2} \end{bmatrix}$$

The control input is reported in the subsequent equation:

$$u = -\left(S\bar{B}\right)^{-1}\left(S\bar{A} - \Phi S + \bar{T}r - \rho\,\mathrm{sign}\left(\sigma\right)\right) \tag{20}$$

C. Attitude controller

Since the payload is modeled as a point mass, the attitude controller, which is the deepest layer of the system, is only responsible for controlling the attitude of the helicopter. The scheme is reported in Fig. 5.

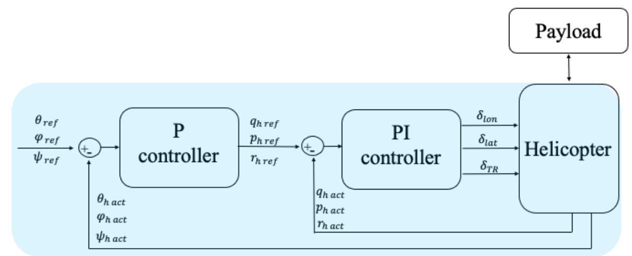

Fig. 5: Helicopter attitude controller

Also the attitude controller is set as a cascade control system [32], in which a primary controller and a primary dynamics are components of the outer loop. The set-points of the inner loop are determined by this outer loop, which also integrates a secondary control loop. Furthermore, the inner loop's dynamics should be substantially quicker than the outer loop's in order to provide satisfactory results. The control system is able to reduce possible interactions and to enhance stability characteristics thanks to this assumption. As a result, the inner loop's gain may be adjusted higher. Measured feedback signals are employed, such as angular rates and attitudes.

The attitude external loop addresses the Euler angles ϕ, θ and ψ. Defining the attitude error signal:

$$\begin{cases} \epsilon_{\alpha h} = \alpha_{hdes} - \alpha_h \\ \epsilon_{\dot{\alpha} h} = \dot{\alpha}_{hdes} - \dot{\alpha}_h \end{cases} \tag{21}$$

where α and $\dot{\alpha}$ stay for the attutide angle and its derivative. The P-PI control output can be written as follows:

$$\begin{cases} \dot{\alpha}_{hdes} = K_{P\alpha}\epsilon_{\alpha h} \\ \delta_{cmd} = K_{P\dot{\alpha}}\epsilon_{\dot{\alpha} h} + K_{I\dot{\alpha}}\int_0^t \epsilon_{\dot{\alpha} h} dt \end{cases} \tag{22}$$

where K_P are the proportional gains and K_I the integral gains.

It has to be mentioned that the reference heading angle does not come directly from the helicopter speed controller. It is directly given to the helicopter from the waypoints generator, which points the helicopter's nose towards the direction of the desired following waypoint.

IV. Results

This section presents the key findings of the simulation campaign, which was conducted to evaluate the controller performance and robustness. The nonlinear system model described in Section II is implemented in the Matlab/Simulink environment. The differential equations are solved by the eight-order Dormand–Prince method [33] with a frequency of 1000 Hz. The UAV used in the simulation is a small-scale remotely piloted helicopter, namely *SAB Goblin Black Thunder 700*, whose characteristics are listed in [34], namely mass and inertia properties, and geometric and aerodynamic data. The payload is a point mass connected to the hook point with a linear-elastic cable. Since the payload is affected by hydrodynamic drag, the frontal reference area $A_p = \pi R_p^2$ of an equivalent sphere is considered. Payload and cable data are given in Tab. I.

TABLE I: Payload and cable relevant parameters

Payload data	Value	Units	
Mass	m_p	0.8	kg
Radius	R_p	0.0505	m
Drag coefficient	C_D	0.47	-
Cable data	**Value**	**Units**	
Length	L	5	m
Hooke's constant	K	4900	N/m
Hook point in Body frame	d_{hp}	[0 0 0.05]	m

It is assumed that payload's density is higher than that of water so that the payload is completely submerged into the water. The control system parameters are tuned by trial and error and are not here reported for the sake of brevity. They can be made available upon request to the reader. To evaluate the effectiveness of control system architecture two simulation cases are presented as follows:

- Speed step test: the aim of this simulation is to show the goodness of the speed controller. A step input is given to payload longitudinal reference velocity. For the purpose of conciseness, step inputs on speed on the other axes are not displayed.
- Waypoints tracking test: the purpose of this simulation is to demonstrate the effectiveness of the controller position. The position controller is asked to track the payload a list of waypoints to show the preciseness of the control architecture.

A. Speed test

In this simulation a step input of $+0.5$ m/s is given to the reference longitudinal velocity after 10 s and then a step input of -0.5 m/s at 30 s. Fig. 6 shows the desired vs the actual velocities of the payload, which highlights that the controller is capable to follow the desired signal. Noteworthy when the payload longitudinal speed changes there is small coupling with payload vertical speed.

Fig. 7,8 display the behaviour of the helicopter speed controller (SMC + PID) and of the helicopter attitude controller. For both, the desired signal is followed by the controller.

B. Waypoints tracking test

In this test case, it is requested to the control system to track a desired set of waypoints WP_i, that are given in Table II, in which the first line coincides with the initial payload position. Each target is assumed to be reached when its distance from the payload is less or equal to 0.5 m. The prescribed set is generated to simulate an actual scenario where the payload can be a sensor that needs to gather data in water at various locations.

Figure 9 shows the desired and the actual trajectories of the payload based on the prescribed set of waypoints. The simulation displays that the payload follows the desired waypoints.

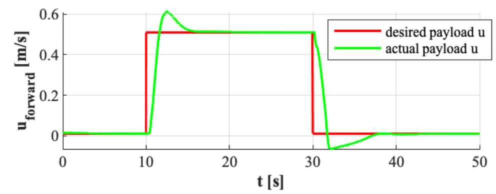

(a) Desired vs actual longitudinal payload speed

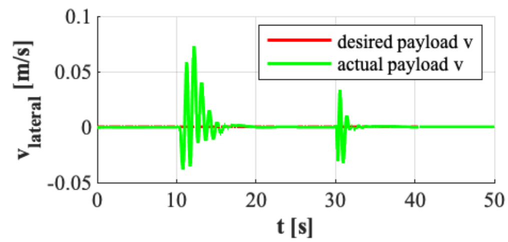

(b) Desired vs actual lateral payload speed

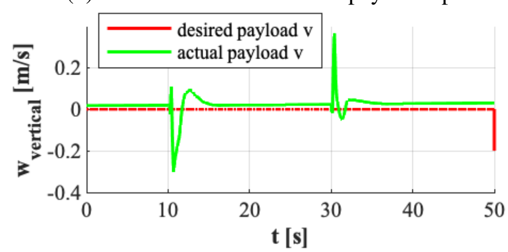

(c) Desired vs actual vertical payload speed

Fig. 6: Desired vs actual payload velocities

i-th waypoint	x_i [m]	y_i [m]	z_i [m]
1	0	0	1
2	20	0	1
3	20	5	1
4	30	5	1
5	30	0	1
6	40	0	1
7	40	-5	1
8	50	-5	1
9	50	0	1

TABLE II: Waypoint list

With the aim to characterize and quantify control system performance, two indicators are defined [35]:

- Maneuver time t_m: it is the amount of time needed to complete a maneuver. For this simulation, each change of waypoint is considered as a single maneuver, so that t_m is the time needed to move from a waypoint to the following one.
- Average trajectory-tracking error $\bar{d}$: it is the error in position computed during each displacement between the waypoints. It is calculated as

$$\bar{d} = \frac{1}{t_m} \int_0^{t_m} d(s)\, ds \tag{23}$$

where $d(t)$ characterizes the precision of displacements for point-to-point placement within the framework of waypoint navigation. Assume A and B are consecutive waypoints, respectively, identified by position vectors p_A and p_B. $d(t)$

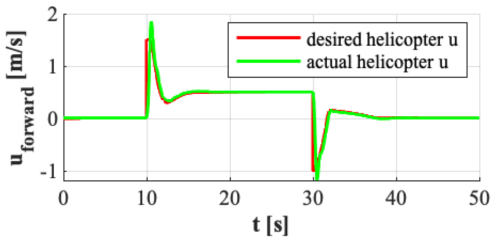

(a) Desired vs actual longitudinal helicopter speed

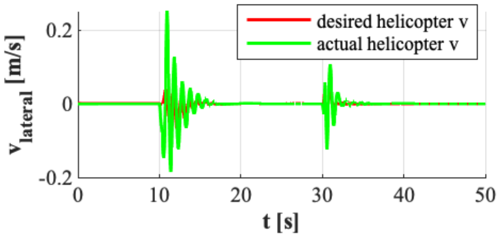

(b) Desired vs actual lateral helicopter speed

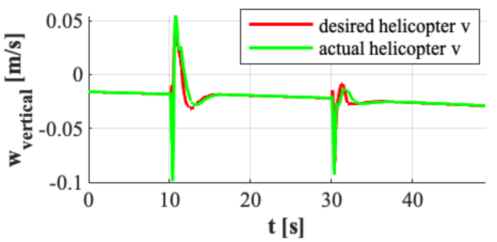

(c) Desired vs actual vertical helicopter speed

Fig. 7: Desired vs actual helicopter velocities

represents the distance at time t of the payload from the direction defined by vector $p_A - p_B$.

Table III summarizes the performance indicators.

i-th waypoint	t_m [s]	$\bar{d}$ [m]
2	30.46	0.032
3	14.94	0.1445
4	43.87	0.059
5	15.16	0.1438
6	57.32	0.1594
7	15.38	0.1432
8	70.73	0.1694
9	30.21	0.0154

TABLE III: Performance indicators

It is noteworthy that the indicator $\bar{d}$ is always under 0.2 m, pointing out the goodness of the controller.

V. Conclusions

In this work, a hierarchical control architecture for a system made by a small-scale remotely-piloted helicopter and a submerged payload is tested through simulation. The simulations are articulated in two main tests: 1) Speed step test; 2) Waypoints tracking test.

The goal of the simulation scenario is to simulate a real-world situation where a UAV is carrying a sensor or a set of sensors as payload for environmental monitoring in an aquatic environment. The control system can precisely

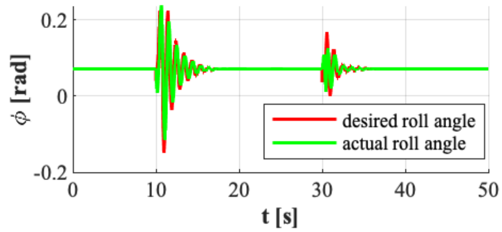

(a) Desired vs actual roll angle

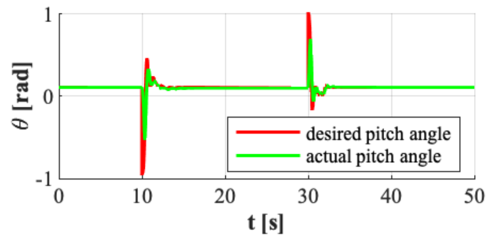

(b) Desired vs actual pitch angle

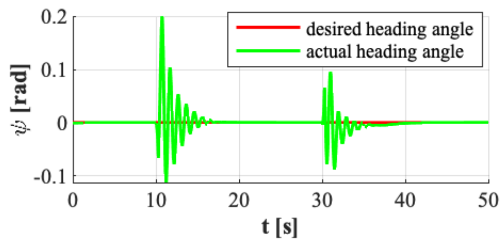

(c) Desired vs actual heading angle

Fig. 8: Desired vs actual helicopter attitude

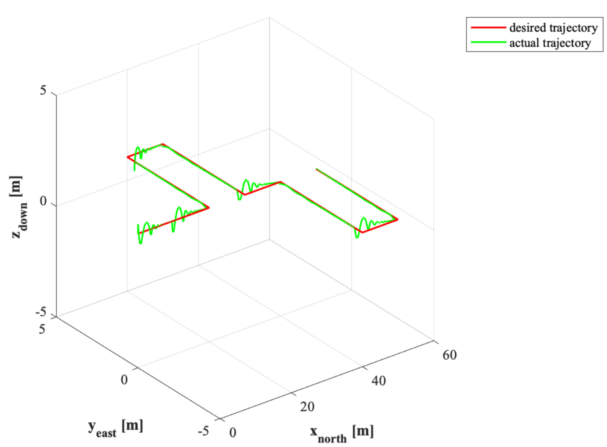

Fig. 9: Trajectory followed by payload vs payload desired trajectory based on the set of prescribed waypoints

monitor reference signals, as demonstrated by the results, in particular the waypoint tracking. Throughout the whole maneuver, a maximum deviation of 0.17 m was found from performance indicators, demonstrating how accurate the position controller is. Although this study may be regarded as preliminary, it shows that hierarchical control schemes may be coupled in an efficient manner to operate a helicopter that is used for environmental monitoring in aquatic situations. The main contribution of this paper is the implementation of a mathematical model of the UAV helicopter-cable-payload system for water monitoring and the design of a proper hierarchical control system. Future work shall focus on the refinement of the models of the payload and of the cable, while adding considerations on the proper stabilization of the payload. Considerations on disturbance rejection will be made. In addition, experimental tests on a real helicopter platform carrying different sensors for water monitoring should be done.

References

[1] S. Manfreda, M. F. McCabe, P. E. Miller, R. Lucas, V. P. Madrigal, G. Mallinis, E. B. Dor, D. Helman, L. Estes, G. Ciraolo, J. Müllerová, F. Tauro, M. I. D. Lima, J. L. M. P. D. Lima, A. Maltese, F. Frances, K. Caylor, M. Kohv, M. Perks, G. Ruiz-Pérez, Z. Su, G. Vico, and B. Toth, "On the use of unmanned aerial systems for environmental monitoring," *Remote Sensing*, vol. 4, no. 641, 2018.

[2] Y. Kaizu, M. Iio, H. Yamada, and N. Noguchi, "Development of unmanned airboat for water-quality mapping," *Biosystems Engineering*, vol. 109, no. 4, pp. 338–347, 2011.

[3] B. A. Schaeffer, K. G. Schaeffer, D. Keith, R. S. Lunetta, R. Conmy, and R. W. Gould, "Barriers to adopting satellite remote sensing for water quality management," *International Journal of Remote Sensing*, vol. 34, no. 21, pp. 7534–7544, 2013.

[4] D. Romić, A. Castrignanò, M. Romić, G. Buttafuoco, M. Bubalo Kovačić, G. Ondrašek, and M. Zovko, "Modelling spatial and temporal variability of water quality from different monitoring stations using mixed effects model theory," *Science of The Total Environment*, vol. 704, p. 135875, 2020.

[5] W. Chen, X. Hao, J. Lu, K. Yan, J. Liu, C. He, and X. Xu, "Research and design of distributed iot water environment monitoring system based on lora," *Information Security Protection Technology in Industrial Internet of Things*, 2021.

[6] C. Peters, Y. Zhan, M. Schwartz, L. Godoy, and H. Ballard, "Trusting land to volunteers: How and why land trusts involve volunteers in ecological monitoring," *Biological Conservation*, vol. 208, pp. 48–54, 2017.

[7] D. Karimanzira, M. Jacobi, T. Pfuetzenreuter, T. Rauschenbach, M. Eichhorn, R. Taubert, and C. Ament, "First testing of an auv mission planning and guidance system for water quality monitoring and fish behavior observation in net cage fish farming," *Information Processing in Agriculture*, vol. 1, no. 2, pp. 131–140, 2014.

[8] H. Lally, I. O'Connor, O. Jensen, and C. Graham, "Can drones be used to conduct water sampling in aquatic environments? a review," *Science of The Total Environment*, vol. 670, pp. 569–575, 2019.

[9] K. Sanim, C. English, Z. B. Kitzhaber, M. Kalaitzakis, N. Vitzilaios, M. L. Myrick, M. E. Hodgson, and T. L. Richardson, "Autonomous uas-based water fluorescence mapping and targeted sampling," *Journal of Intelligent Robotic Systems*, vol. 108, no. 25, 2023.

[10] K. A. Wójcik, R. Bialik, M. Osińska, and M. Figielski, "Investigation of sediment-rich glacial meltwater plumes using a high-resolution multispectral sensor mounted on an unmanned aerial vehicle," *Water*, vol. 11, no. 11, 2019.

[11] J. Chen, Z. Li, L. Li, J. Wang, W. Qi, C. Y. Xu, and J. Kim, "Evaluation of multi-satellite precipitation datasets and their error propagation in hydrological modeling in a monsoon-prone region," *Remote Sensing*, vol. 12, no. 21, 2020.

[12] S. Caldwell, C. Kelleher, E. Baker, and L. Lautz, "Relative information from thermal infrared imagery via unoccupied aerial vehicle informs simulations and spatially-distributed assessments of stream temperature," *Science of The Total Environment*, vol. 661, no. 21, pp. 364–374, 2019.

[13] G. Avanzini, F. Liberati, and G. D. Matteis, "Inverse simulation of a helicopter-towing cable-sonar system," in *45th European Rotorcraft Forum*, September 2019.

[14] X. Cui, Y. Wang, S. Yang, H. Liu, and C. Mou, "Uav path planning method for data collection of fixed-point equipment in complex forest environment," *Frontiers in Neurorobotics*, vol. 16, 2022.

[15] A. Davis, P. S. Wills, J. Garvey, W. Fairman, M. Karim, and B. Ouyang, "Developing and field testing path planning for robotic aquaculture water quality monitoring," *Applied Science*, vol. 13, 2023.

[16] R. Zhang, Z. Wang, X. Li, Z. She, and B. Wang, "Water quality sampling and multi-parameter monitoring system based on multi-rotor uav implementation," *Water*, vol. 15, no. 11, 2023.

[17] C. Koparan, A. B. Koc, C. V. Privette, and C. B. Sawyer, "In situ water quality measurements using an unmanned aerial vehicle (uav) system," *Water*, vol. 10, no. 3, 2018.

[18] M. Schwarzbach, K. Kondak, M. Laiacker, C.-Y. Shih, and P. J. Marrón, "Helicopter uav systems for in situ measurements and sensor placement," in *2012 IEEE International Geoscience and Remote Sensing Symposium*, 2012, pp. 4766–4769.

[19] A. Sridharan, "Simulation modeling of flight dynamics, control and trajectory optimization of rotorcraft towing submerged loads," Ph.D. dissertation, University of Maryland, 2014.

[20] G. Guglieri and M. Paolo, "Dynamic stability of a helicopter with an external suspended load," *Journal of the American Helicopter Society*, vol. 59, no. 4, 2014.

[21] L. Liu, M. Chen, T. Li, and H. Wang, "Composite anti-disturbance reference model l2 linf control for helicopter slung load system," *Journal of Intelligent & Robotic Systems*, vol. 102, pp. 1–21, 2021.

[22] Y. Ren, M. Chen, and J. Liu, "Unilateral boundary control for a suspension cable system of a helicopter with horizontal motion," *IET Control Theory & Applications*, vol. 13, no. 4, pp. 467–476, 2019.

[23] K. Thanapalan, "Nonlinear controller design for a helicopter with an external slung load system," *Systems Science & Control Engineering*, vol. 5, no. 1, pp. 97–107, 2017.

[24] Y. Cao and Z. Wang, "Equilibrium characteristics and stability analysis of helicopter slung-load system," *Proceedings of the Institution of Mechanical Engineers, Part G: Journal of Aerospace Engineering*, vol. 231, no. 6, pp. 1056–1064, 2017.

[25] G. Bertolani, A. D. Ryals, E. L. de Angelis, and F. Giulietti, "Hierarchical dual-loop speed control for a helicopter," in *49th European Rotorcraft Forum*, September 2023.

[26] T. L. Heath, *The works of archimedes*. Cambridge: Cambridge University Press Warehouse, 1897.

[27] P. D. Talbot, B. E. Tinling, W. A. Decker, and R. T. N. Chen, "A mathematical model for a single main rotor helicopter for piloted simulation," Sept. 1982, ames Reasearch Center, Moffett, Field, California.

[28] D. A. Peters and N. HaQuang, "Dynamic inflow for practical applications," *Journal of the American Helicopter Society*, vol. 33, no. 4, pp. 64–68, 1988.

[29] J. G. Leishman, *Principles of helicopter aerodynamics*, ser. Cambridge aerospace series 12. Cambridge: Cambridge University Press, 2000.

[30] R. T. N. Chen, "A simplified rotor system mathematical model for piloted flight dynamics simulation," May 1979, ames Reasearch Center, Moffett, Field, California.

[31] R. Heffley and M. A. Mnich, "Minimum complexity helicopter simulation math model," April 1988, ames Reasearch Center, Moffett, Field, California.

[32] G. Szafranski and C. Roman, "Different approaches of pid control uav type quadrotor," in *The international micro air vehicles conference*, 2011, pp. 70–75.

[33] J. R. Dormand, *Numerical Methods for Differential Equations: A Computational Approach*. CRC Press, 1996.

[34] G. Bertolani, A. D. Ryals, F. Giulietti, and L. Pollini, "$\mathcal{L}_1$ adaptive speed control for a helicopter," in *48th European Rotorcraft Forum*, September 2022.

[35] E. L. de Angelis and F. Giulietti, "An improved method for swing state estimation in multirotor slung load applications," *Drones*, vol. 7, no. 11, 2023.